Preprints (www.preprints.org) | NOT PEER-REVIEWED | Posted: 19 October 2018 doi:10.20944/preprints201810.0441.v1

Peer-reviewed version available at J. Mar. Sci. Eng. 2018, 6, 155; doi:10.3390/jmse6040155

*Article*

# On the effect of cavity formation during the water entry of flexible bodies

**Riccardo Panciroli [1,*], Tiziano Pagliaroli [1] and Giangiacomo Minak [2]**

[1] Niccolò Cusano University, via don Carlo Gnocchi 3, Rome, Italy
[2] Alma Mater Stuiorum - Università di Bologna, DIN, via Fontanelle 40, Forlì, Italy
* Correspondence: riccardo.panciroli@unicusano.it

**Abstract:** Elastic bodies entering the water might experience Fluid-Structure Interaction phenomena introduced by the mutual interaction between the structural deformation and the fluid motion. Cavity formation, often misleadingly named cavitation, is one of these. This work presents the results of an experimental investigation on the water entry of deformable wedges impacting a quiescent water surface with pure vertical velocity in free fall. The experimental campaign is conducted on flexible wedges parametrically varying the flexural stiffness, deadrise angle, and drop height. It is found that under given experimental conditions cavity pockets forms beneath the wedge. Their generation mechanism is found to be ruled by a differential between structural and fluid velocities, which is introduced by the structural vibrations. Results show that the impact force during water entry of stiff bodies is always opposing gravity, while in case of flexible bodies might temporarily reverse its direction, with the body that is being sucked into the water within the time frame between the cavity formation and its collapse. Severe impacts might also generate a series of cavity generation and collapses.

**Keywords:** Water Entry, hydroelasticity, cavitation, FSI, SPH, slamming

## 1. Introduction

The impulsive nature of the hydrodynamic loading experienced by structures impacting the water might induce mechanical vibrations [1–3]. These introduce a series of so-called fluid-structure interaction (FSI) phenomena, such as air inclusions [4], ventilation, and cavitation [5], which are encountered in a wide range of water entry problems from naval [6–9] to aerospace applications [10–12]. In the literature, many experimental works investigated the hydrodynamic pressure at the fluid-structure interface during the water entry of rigid or very stiff bodies, showing that established analytical formulations [13,14] can be used with very high confidence [15]. However, in case of FSI, the theoretical formulations capable of predicting the hydrodynamic impact load developed for the water entry of rigid bodies become inaccurate. Due to the mutual coupling between the fluid motion and the structural deformation, the hydrodynamic loads that elastic bodies are subjected during the water entry might differ from the loads acting on rigid bodies [16]. The evolution of the wetted body area in time is an important characteristic of the impact, and variations of the structural shape due to its flexibility might affect the loads [17]. Such problems are still difficult to analyse and compute. Predicting the structural deformations and stresses during the water entry of flexible structures is a major challenge and a deep understanding of these FSI phenomena is a dire need. Most of the analytical and numerical works found in the literature [18–21] do not account for such FSI phenomena, since these can be neglected in the cases where structural deformations are small and the hydrodynamic pressure is similar to the one experienced by a rigid body (see e.g. [22–25]).

© 2018 by the author(s). Distributed under a Creative Commons CC BY license.

Preprints (www.preprints.org) | NOT PEER-REVIEWED | Posted: 19 October 2018 doi:10.20944/preprints201810.0441.v1

Peer-reviewed version available at J. Mar. Sci. Eng. 2018, 6, 155; doi:10.3390/jmse6040155



The occurrence of cavitation during the water entry of flexible bodies has been predicted in the literature (e.g. [7,26]). Hydroelasticity might facilitate cavitation [6,27], since pressure becomes sub-atmospheric during the second half of the first wet natural oscillation period. Reinhard [28] analytically predicted that there are conditions for which a wedge entering the water in free fall might form a cavity localized at its apex. Therein, the authors also mention that elasticity of the structure might enhance such phenomenon. In the literature, the term cavitation is often misused, as many works relative to water entry problems use this term to define the generation of cavity formation, rather than effective cavitation in its original meaning [29,30]. Korobkin [26] predicted that in blunt bodies subjected to a sudden velocity drop the liquid may separate from the entering body surface with formation of a cavity. He defined this phenomenon as interface cavitation. In his model, which bases on Wagner's [13] theory, the cavitation is supposed to happen when the local pressure goes below the atmospheric. During the water entry of flat–bottom bodies, or geometries presenting low deadrise angle, air can be trapped in between the fluid and the structure during the early stage of the impact [31–34]. In such occurrence an air cushion is entrapped below the structure, lowering the hydrodynamic loading. Furthermore, the presence of entrapped air in the fluid is supposed to inhibits cavitation.

In this work we report on experimental evidences about cavity formation during water entry of flexible structures. Many experimental campaigns on the water impact of compliant bodies can be found in the literature [35–38], but to the Authors' best knowledge, none of these reported on cavity formation. The following sections report the most important experimental findings. At first, we give some insight on the analytical prediction of cavitation during the water entry of rigid bodies, showing the actual possibility of such effect. We then present the experimental setup, followed by some details about the experimental results. The effects of cavity formation on the impact dynamics are presented hereafter.

## 2. Cavitation onset in rigid bodies water entry as predicted by analytical formulations

The dynamics of the water entry of rigid bodies can be accurately predicted by utilizing Wagner's model [13]. Such solution relies on the concept of added mass (or virtual mass), where an increasing mass $m$ of water is considered to move with the body as it penetrates the water. In this framework, the velocity and acceleration of the impacting wedge are given by [13]

$$\dot{\xi} = \frac{MV_0}{M+m} = \frac{V_0}{1+\frac{\pi}{2}\rho\frac{(\pi/2)^2\xi^2}{M\tan^2(\beta)}} \qquad \ddot{\xi} = \frac{\mathrm{d}}{\mathrm{d}t}\frac{MV_0}{M+m} = \frac{\pi\rho(\pi/2)^2}{MV_0\tan^2(\beta)}\xi\dot{\xi}^3 \tag{1}$$

being $\xi$ the entry depth, $M$ the mass of the wedge per unit depth, $V_0$ the initial entry velocity, and $\beta$ the deadrise angle. Figure 1 shows a sketch of the problem. Wagner's model further allows to compute the pressure distribution along the wet portion of the body as

$$\frac{p}{\rho} = \ddot{\xi}\sqrt{r^2-x^2} + \frac{\pi}{2}\frac{\dot{\xi}^2 r}{\tan(\beta)\sqrt{r^2-x^2}} - \frac{1}{2}\frac{\dot{\xi}^2 x^2}{r^2-x^2} \tag{2}$$

where $r$ is the horizontal projection of the wet length of the wedge, which reads $\frac{\pi}{2}\frac{\xi}{\tan\beta}$. The factor $\frac{\pi}{2}$ accounts for the water pile-up along the wetting edge due to the displaced water. Such value has been later found not to be a constant, as it actually varies with the deadrise angle [39]. We'll here utilize $\frac{\pi}{2}$ as this does not qualitatively alter the solution.

In the case of water entry at a constant speed, the solution is self-similar in time. Otherwise, the component related to the acceleration may overcome the component associated to the velocity in equation (2), with the pressure eventually going sub-atmospheric at some locations.

Preprints (www.preprints.org) | NOT PEER-REVIEWED | Posted: 19 October 2018 doi:10.20944/preprints201810.0441.v1

Peer-reviewed version available at J. Mar. Sci. Eng. 2018, 6, 155; doi:10.3390/jmse6040155



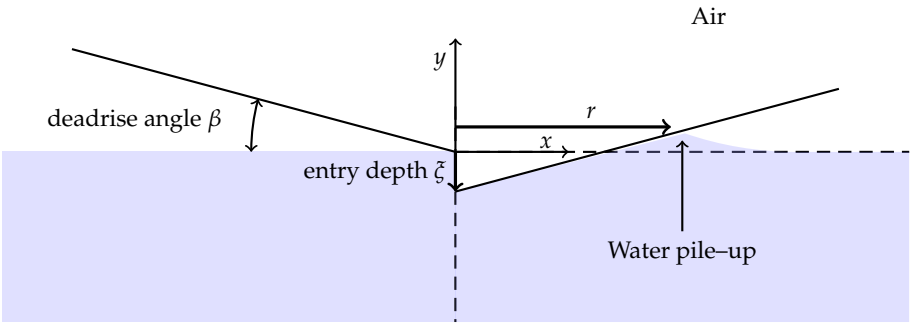


**Figure 1.** Sketch of the problem of the water entry of a rigid wedge. The wedge enters the water surface at $t = 0$ (left) and penetrates the water by an entry depth $\xi$ as time advances (right).

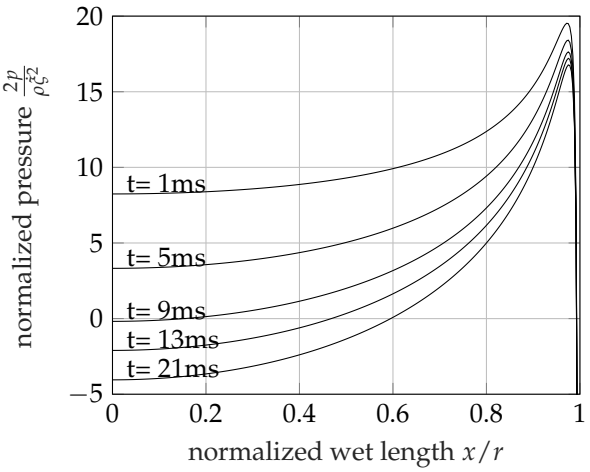


**Figure 2.** Wagner's predicted normalized pressure as a function of the normalized wet length $x/r$ at several instants. Solution calculated for a wedge weighting 5kg/m, 20° deadrise angle, and entering the water at 2m/s with pure vertical velocity.

Figure 2 shows an example Wagner's pressure distribution prediction at several impact times. The location of the peak pressure is constant and the minimum pressure is always located at the keel of the wedge ($x = 0$), and equals

$$p_{\text{keel}} = \frac{1}{2}\rho\dot{\xi}^2\pi\cot(\beta) + \ddot{\xi}\rho r \tag{3}$$

We can therefore express the cavitation onset condition in terms of the dynamics components as

$$\dot{\xi}^2 + \ddot{\xi}\xi < (p_{\text{v}} - p_{\text{a}})\frac{2\tan(\beta)}{\pi\rho} \tag{4}$$

being $p_{\text{a}}$ the atmospheric pressure and $p_{\text{v}}$ the vapour pressure. Using equation (1), the left hand side of the formula can be written in terms of $\xi$ only and equals

$$4\,\frac{\tan^4\beta\, M^2\, V_0{}^2\left(-\pi\rho\gamma^2\xi^2 + 2M\tan^2\beta\right)}{\left(2M\tan^2\beta + \pi\rho\gamma^2\xi^2\right)^3} \tag{5}$$

Preprints (www.preprints.org) | NOT PEER-REVIEWED | Posted: 19 October 2018 doi:10.20944/preprints201810.0441.v1

Peer-reviewed version available at J. Mar. Sci. Eng. 2018, 6, 155; doi:10.3390/jmse6040155



showing a minimum at the entry depth $\xi^* = 4\frac{\sqrt{\pi\rho M}\tan(\beta)}{\pi^2\rho}$ which, substituted in eq. 4, predicts that the minimum pressure at the keel is

$$\dot{\xi}^2 + \ddot{\xi}\xi\Big|_{\xi^*} = -\frac{1}{27}V_0^2 \tag{6}$$

It is noticeable that the penetration depth $\xi^*$ might not be reached during the impact due to insufficient initial entry velocity. Wagner's solution thus predicts that cavitation during the water entry of a rigid wedge occurs if

$$-\frac{1}{27}V_0^2 < (p_v - p_a)\frac{\tan(\beta)}{\frac{\pi}{2}\rho} \tag{7}$$

Notably, $\xi^*$ is independent from the impact velocity but is function of the geometrical data only. Figure 3 (left) shows the normalized pressures versus the entry depth for various deadrise angles.

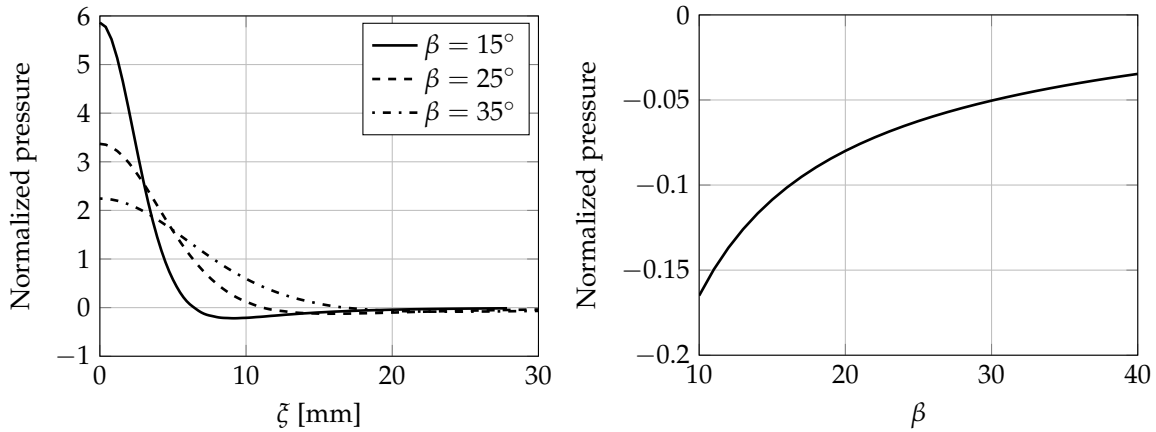


**Figure 3.** Left: Normalized pressure versus entry depth for varying deadrise angles. Right: Normalized minimum pressure versus deadrise angle.

If we concentrate on the minimum value of the normalized pressure we see that this increases with the deadrise angle, as displayed in figure 3 (right). Here, only deadrise angles higher than 10° are shown, as lower values are known to lead to the so–called air trapping phenomenon [4], that is, some air is entrapped in between the structure and the fluid during the water entry to form an air cushion, decreasing the impact load and inhibiting cavitation.

## 3. Preliminary experimental evidences

The analytical solution presented in the previous section shows that cavitation (intended in its original meaning) do might appear during the water entry of rigid bodies. However, such occurrence is extremely difficult to be attained as to reach pressures lower than the vapour pressure we need the combination of very high velocity and extremely lightweight bodies. Similar results were considerations are found in [28] for different body shapes. Further, all these solutions are 2D approximations and do not take into account for the effects at the front and rear faces of the wedge (but are indeed valid for axial-symmetric bodies). We will now discuss such issue by referring to the keel edge only, being the location where the minimum pressure is attained. The keel is always wet, being the first portion of the wedge touching the water. However, as the wedge enter the water, it digs a hole on it, pushing the water sideways. The front and back sides of the wedge actually remain dry and always "see" the atmospheric pressure. The hole in the water will eventually collapse, but it takes a time way longer than the impact duration. Therefore, the pressure at the keel varies from the theoretical one at its mid-span to the atmospheric one at its vertexes. As the pressure at keel goes below the gage pressure, its effect is forcing some air to enter from the sides, forming a cavity beneath the wedge.

Preprints (www.preprints.org) | NOT PEER-REVIEWED | Posted: 19 October 2018 doi:10.20944/preprints201810.0441.v1

Peer-reviewed version available at J. Mar. Sci. Eng. 2018, 6, 155; doi:10.3390/jmse6040155



We performed some experiments on rigid wedges on this sense. In our experience such occurrence never happened in free-fall impacts, but was indeed found when the deceleration of the wedge was imparted mechanically through a pneumatic actuator, or by a mechanic end-run forcing the wedge to suddenly decelerate. Such results are thus to be considered artificial and are not presented here. We therefore never encountered cavity formation in free fall water entry of rigid bodies, whereas we indeed found it in case of free fall impacts of flexible bodies. The following sections will introduce the most important results about cavity formation during the water entry of flexible wedges.

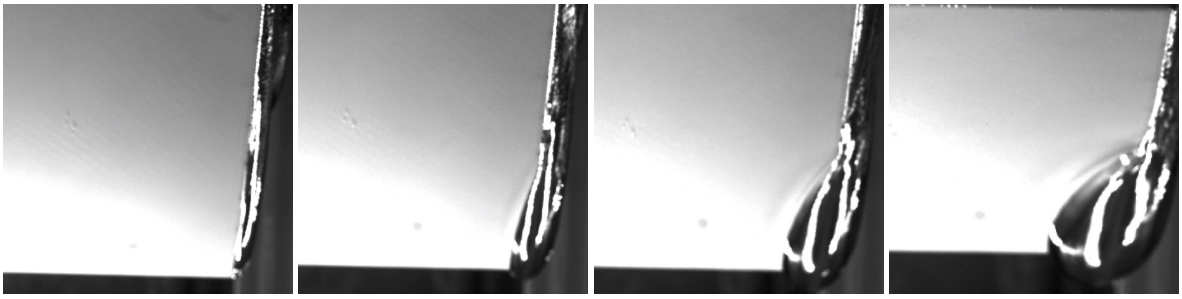

**Figure 4.** Details of the vertex of the keel at several time instants, presenting the evolution of the cavity formation. Images are taken from the side.

Figure 4 shows the evolution of a cavity formation in the neighbourhood of the vertex of the keel of a wedge. The cavity formation mechanisms is equally generating on both the wedge vertexes and only one of these is reported in the images for convenience. The images are presented here with the sole intent of explaining the mechanism of cavity formation during water entry as these do not refer to the present experimental campaign, since the experimental apparatus utilized in this work does not allow to capture images from the lateral view, but from the front side only.

## 4. Experimental set-up

Experiments were conducted on a drop weight apparatus appositely assembled for the experimental campaign. The falling body is comprised by a sledge holding two panels joined together by a tunable hinge to form a v-shaped object. The deadrise angle $\beta$ may range smoothly from $0^\circ$ to $50^\circ$. The hinge holds the panels in a cantilever configuration in a clamped-free boundary condition. Experiments have been conducted on bodies with a sufficiently large deadrise angle ($> 10^\circ$) to avoid air bubbles inclusions [4].

The experimental setup is the same utilized in [40]. Impact acceleration is measured by a *V-Link Microstrain* wireless accelerometer ($\pm 100g$) located at the tip of the wedge. All reported accelerations are referenced to 0 $g$ for the free-falling phase. The sampling frequency is set to its maximum of 4kHz. Entering velocity is recorded by a laser sensor ($\mu\epsilon$ ILS 1402) capturing the sledge position over 350mm of ride at a frequency of 1.5kHz with a resolution of 0.2mm. The entry velocity is obtained through central difference of the position signal.

The dynamics of the impact is captured through a high speed camera looking trough a window on the water tank. As mentioned before, only frontal views can be captured through the high speed camera in the present experimental apparatus. The capturing frequency is set to 4 kHz with a definition of 1280x800px. A vertical clear screen has been placed inside the water tank just before the wedge preventing fluid spraying in the axial direction. The clearance between the screen and the falling body is about 2mm, but it slightly vary during the water entry due to the varying fluid pressure moving and deforming the screen. The use of the screen is necessary to see the evolution of the fluid jet (pileup) rising on the sides of the wedge, and to prevent fluid spraying through the camera which would affect the visibility of the image.

Preprints (www.preprints.org) | NOT PEER-REVIEWED | Posted: 19 October 2018 doi:10.20944/preprints201810.0441.v1

Peer-reviewed version available at J. Mar. Sci. Eng. 2018, 6, 155; doi:10.3390/jmse6040155



### 4.1. Specimens

Hydroelastic effects are influenced by the ratio between the wetting time and the panel's lower natural frequency [6,41]. To vary the fundamental natural frequency of the panels, different stiffness to area density ratios have been utilized: Aluminum (A), E-glass (mat) / vinylester (V), and E-Glass (woven) / epoxy (W) 2mm and 4mm thick were used. All wedges are made by two panels 300mm long and 250mm width. Aluminum and composite panels material properties are listed in table 1. Composite panels were produced by VARTM by infusion of vinylester resin on E-Glass fibre mat, while the E-glass (woven $0°/90°$) / epoxy panels were produced in autoclave. The first three dry vibration frequencies of the panels are listed in table 2.

**Table 1.** Material properties.

| Material | Abbr. | $E_1 = E_2$ | $\nu_{12}$ | $\rho[kg/m^3]$ |
|---|---|---|---|---|
| 6068 T6 | A | 68.0 GPa | 0.32 | 2700 |
| E-Glass/Vinylester | V | 20.4 GPa | 0.28 | 2050 |
| E-Glass/Epoxy | W | 30.3 GPa | 0.28 | 2015 |

All panels were equipped with two strain gauges per side, located at 25mm and 120mm from the reinforced tip. The reinforced tip is 27mm long and is used to connect the two panels to the aluminum sledge.

**Table 2.** First three theoretical dry natural frequencies of the panels composing the wedges.

| Abbr. | Material | Thickness | $\omega_1$ [Hz] | $\omega_2$ [Hz] | $\omega_3$ [Hz] |
|---|---|---|---|---|---|
| A2 | aluminum | 2.0 mm | 18.0 | 112.8 | 316.1 |
| A4 | aluminum | 4.0 mm | 36.0 | 225.7 | 632.2 |
| V2 | Fibreglass | 2.0 mm | 9.7 | 61.2 | 171.4 |
| V4 | Fibreglass | 4.0 mm | 19.7 | 123.6 | 346.2 |
| W2 | Fibreglass | 2.2 mm | 19.6 | 123.4 | 345.5 |
| W4 | Fibreglass | 4.4 mm | 37.8 | 236.9 | 663.4 |

A very high number of drop tests have been conducted [42], but high speed imaging has been performed on selected configurations only at the end of the experimental campaign, when the camera has been rented for the purpose. We here therefore report on a limited number of experiments, which are considered to be sufficient to qualitatively describe the effect of cavity formation on the impact dynamics.

## 5. Experimental results

In the following sections the results from the high speed camera are presented. A coupled FEM/SPH numerical model is then utilized to gain deeper knowledge on the fluid-structure interaction phenomena introduced by the structural deformation.

### 5.1. Wedges deformations during the water entry

In a previous research by the authors [41] it was shown that hydroelastic effects in the present experiments is ruled by a parameter $R$, which is proportional to the ratio between the impact time and the first structural natural period. Results showed that the maximum impact–induced stress decreases if compared to the theoretical quasi–static solution when $R$ is lower than 100. Above this value the structural response can be accurately predicted by a quasi–static approach. However, for values of $R$ lower than 100 interesting Fluid-structure interaction phenomena might appear, such as ventilation and cavity formation.

Experiments on elastic wedges with high deadrise angle entering the water at low velocity (R>100) show that the panels are initially slightly deforming downwards (thus showing a convex shape), to later deform upward due to the hydrodynamic pressure. This initial convex deformation has to be

Preprints (www.preprints.org) | NOT PEER-REVIEWED | Posted: 19 October 2018 doi:10.20944/preprints201810.0441.v1

Peer-reviewed version available at J. Mar. Sci. Eng. 2018, 6, 155; doi:10.3390/jmse6040155



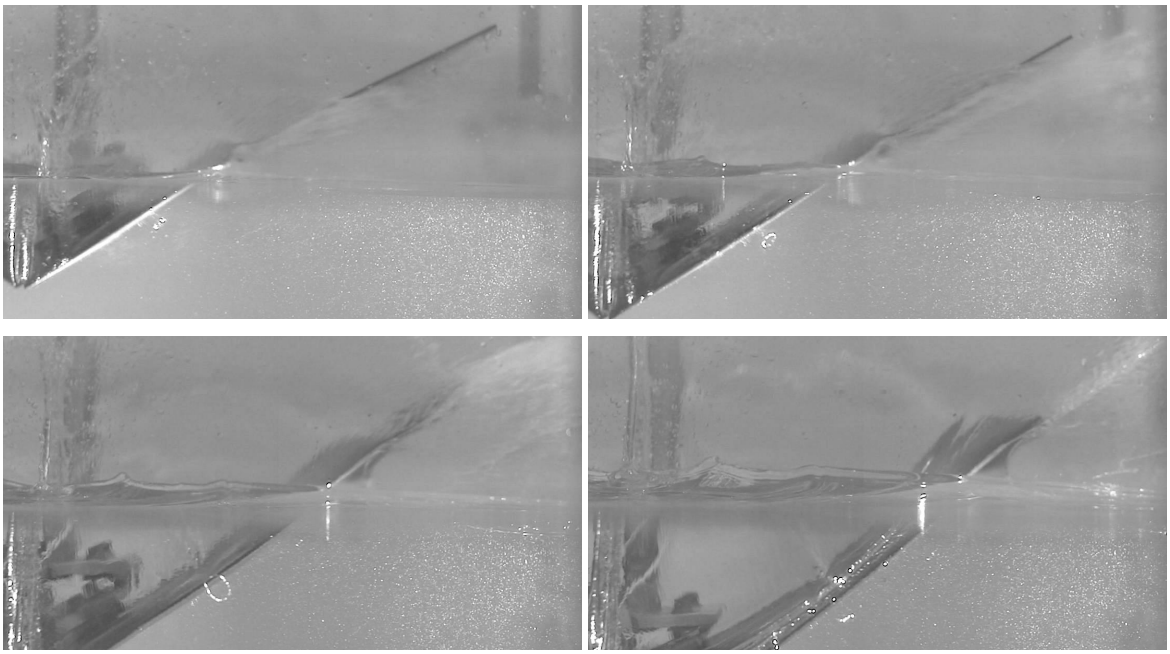

**Figure 5.** Deformation over time of a fibreglass/vinylester wedge with deadrise angle of 30° entering the water at 4.2 m/s.

attributed to the effect of inertia: the hydrodynamic load acts on the wedge apex at first, leading the free edge to deform downwards. As the wedge enters the water the hydrodynamic load covers a larger area and the deformation due to the pressure exceeds the deformation due to inertia, leading the panel to deform upwards. As an example, figure 5 shows the deformation in time of a flexible wedge ($\beta = 30°$) entering the water at 4.2 m/s.

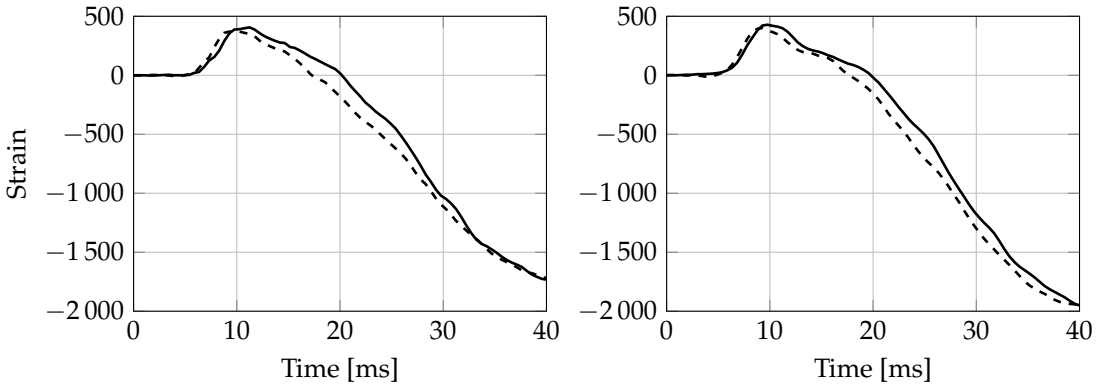


**Figure 6.** Signal recorded by two strain gauges during the water entry of a fiberglass/polyester wedge 4mm thick with deadrise angle of 35° entering the water from an impact height of 1.5m (approx 5m/s). The graph on the right shows the strain measured at the center of the panel, while the graph on the left shows the strain close to the wedge tip. The full and the dashed lines represents two repetitions of the same experiment.

The strains at the vertex and at the middle of the panel assume a shape similar to those presented in figure 6, which shows the example of a fiberglass/polyester wedge 4mm thick with deadrise angle of 35° impacting from an impact height of 1.5m. Generally speaking, in all these cases the panels are deforming downward for a very short portion of the total impact time, and the maximum positive

Preprints (www.preprints.org) | NOT PEER-REVIEWED | Posted: 19 October 2018 doi:10.20944/preprints201810.0441.v1

Peer-reviewed version available at J. Mar. Sci. Eng. 2018, 6, 155; doi:10.3390/jmse6040155



strain (hence the stress) is way lower than the maximum negative strain reached later, revealing that in case of "soft" impact the influence of plates inertia is negligible.

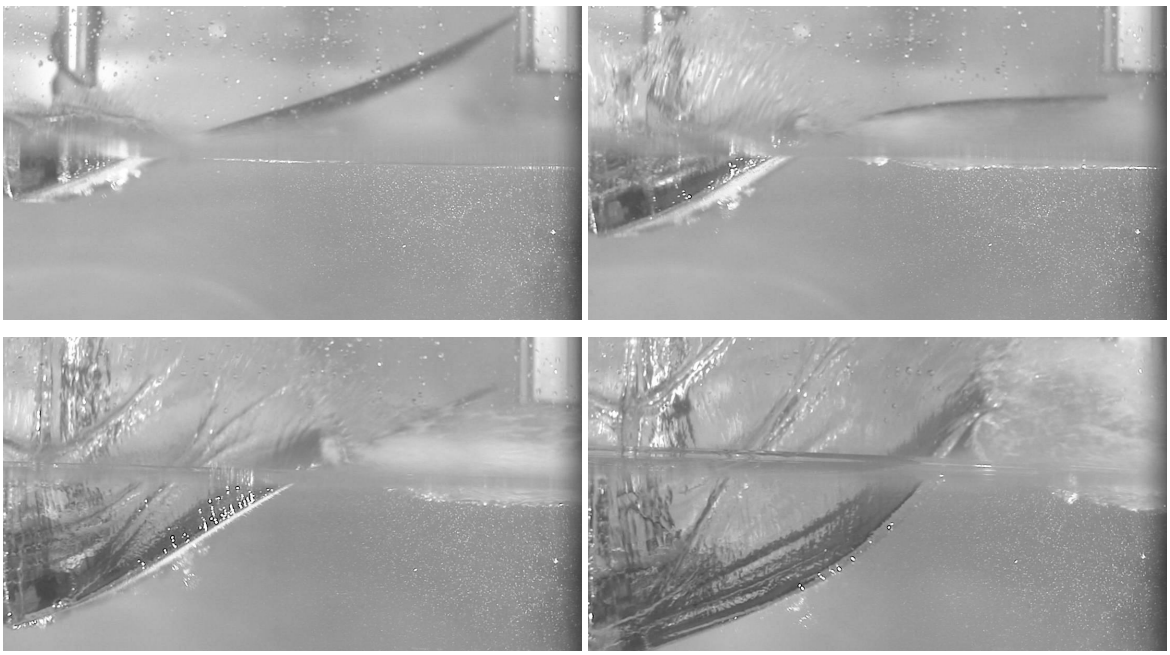

**Figure 7.** Deformation over time of a fibreglass/vinylester wedge 2mm thick with deadrise angle of 20° entering the water at 6.7 m/s.

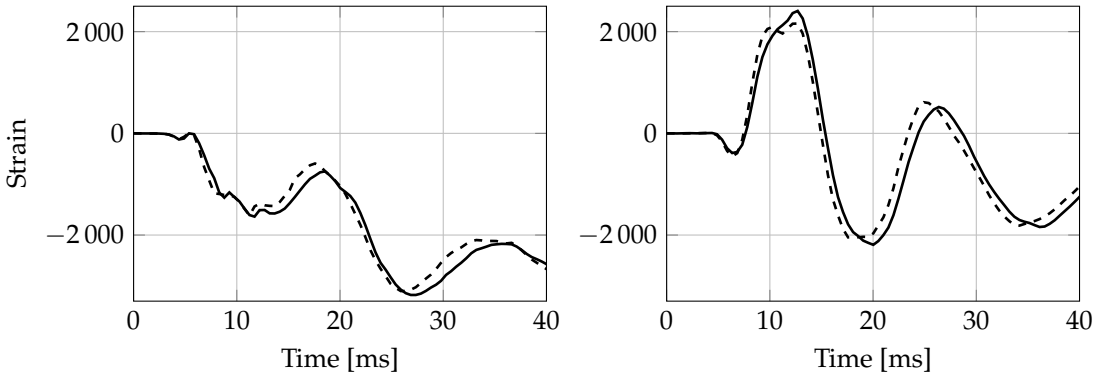


**Figure 8.** Signal acquired by two strain gauges during the water entry. The graph on the right shows the strain measured at the center of the panel, while the graph on the left shows the strain close to the wedge tip. Full and dashed lines are two repetitions of the same experiment.

Conversely, moving to a stronger impact (R<100, by lowering deadrise angle and panel stiffness, and increasing the impact velocity), the dynamic response shows very different results. Figure 7 shows the deformation in time of a flexible wedge entering the water from an impact height of 2.5m. Due to the flexibility of the wedge and the very severe impact load, the panel is largely deforming downward at the beginning of impact. At its maximum deformation (top-right figure) the panel is almost horizontal at its free edge.

The overall deformation of the panels can be better caught by looking at the recordings of the strain gauges, reported in figure 8. The two graphs show that the strain acquired by the gauge close to the wedge tip (left graph) is always negative, indicating a local convex deformation, while the strain gauge at the middle of the panel (right graph) is initially positive (suggesting that the deformation is locally concave), thus leading the panel free edge to deform downward at first. Note that in this

Preprints (www.preprints.org) | NOT PEER-REVIEWED | Posted: 19 October 2018 doi:10.20944/preprints201810.0441.v1

Peer-reviewed version available at J. Mar. Sci. Eng. 2018, 6, 155; doi:10.3390/jmse6040155



case the maximum tensile stress, which is ruled by inertia, is in the same order of magnitude of the compressive stress, which is ruled by the hydrodynamic load. It is thus necessary to consider the effect of inertia in the initial stages of the impact.

### *5.2. Evidences of cavity formation from the high speed images*

It has been mentioned before that increasing the severity of the impact increases the panels deformation. The high speed images captured during the impact showed that the increasing deformation serves as onset for the generation of cavities within the liquid. It was found that in the most severe impacts, after the maximum concave deformation is reached, a clearly visible cylindrical front of cavitating fluid is formed. Figures 9 to 12 show some examples of this phenomenon. Please note that the cylindrical cavity does not extend along the entire width of the wedge, but is concentrated at the front and back edges only, as shown in Section 3.

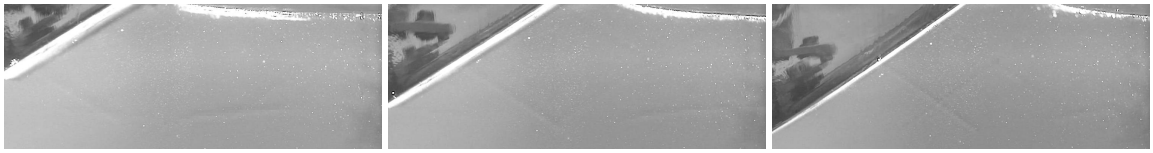

**Figure 9.** Evolution of the water entry of a wedge (W) ($\beta = 30°$) entering the water at ≈4.2 m/s.

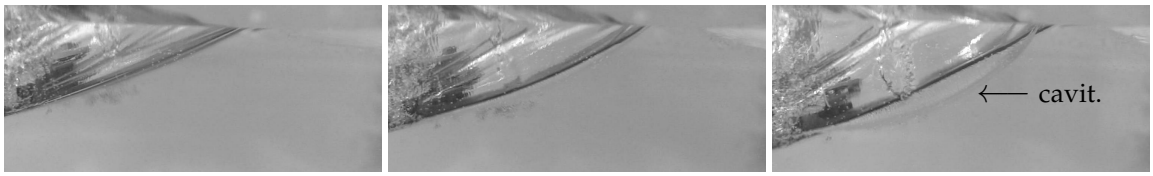


**Figure 10.** Evolution of the water entry of a wedge (W) ($\beta = 15°$) entering the water at ≈6.7 m/s. The arrow highlights the cylindrical front of the cavitating area.

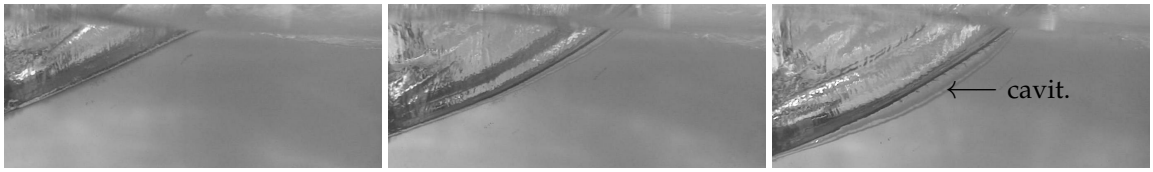


**Figure 11.** Evolution of the water entry of a wedge (V) ($\beta = 20°$) entering the water at ≈4.3 m/s. The arrow highlights the cylindrical front of the cavitating area.

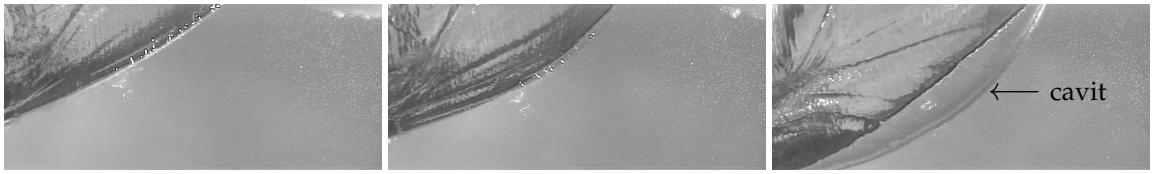


**Figure 12.** Evolution of the water entry of a wedge (V, $\beta = 20°$) entering the water at ≈6 m/s. The arrow highlights the cylindrical front of the cavitating area.

Figure 9 is taken as reference. It shows a wedge with 30° deadrise angle entering the water at 4.3m/s. In this case the deformation of the panels is very low and all the pictures show a smooth and uniformly colored water region. As the severity of the impact increases it is found that a fluid region with cylindrical waveform front generates in the fluid (right pictures in figures 11 to 12). Such

Preprints (www.preprints.org) | NOT PEER-REVIEWED | Posted: 19 October 2018 doi:10.20944/preprints201810.0441.v1

Peer-reviewed version available at J. Mar. Sci. Eng. 2018, 6, 155; doi:10.3390/jmse6040155



phenomenon is always found to develop after the maximum concave deformation is attained (central pictures). We comment that the cavity shape is not in line with the analytical predictions, as it does not seem to originate at the keel, which is the location of minimum pressure. The cavity will eventually collapse during the water entry. In the most severe impacts cases, successive pockets (with decreasing amplitude) might generate and collapse.

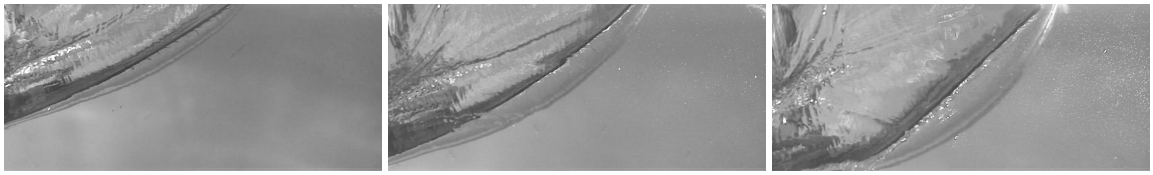

**Figure 13.** Maximum dimension of the wavefront during the water entry of a wedge (V, $\beta = 20°$) entering the water at 4.3, 6, and 6.7 m/s.

Figure 13 shows that for a given wedge (V, $\beta = 20°$) the maximum dimension of the wavefront increases with the impact velocity, as so does the maximum deformation. Please note that the images in figure 13 correspond to the same impact time. In fact, as mentioned before, the cavity formation phenomena initiates after the maximum deformation of the wedge is reached; such deformation is ruled by the first natural frequency of the panel, which is not influenced by the entry velocity.

It was previously shown that the cavity cross-sectional area increases with the impact velocity and structural compliance. We here give some insights on its effect on the acceleration of the body during the impact.

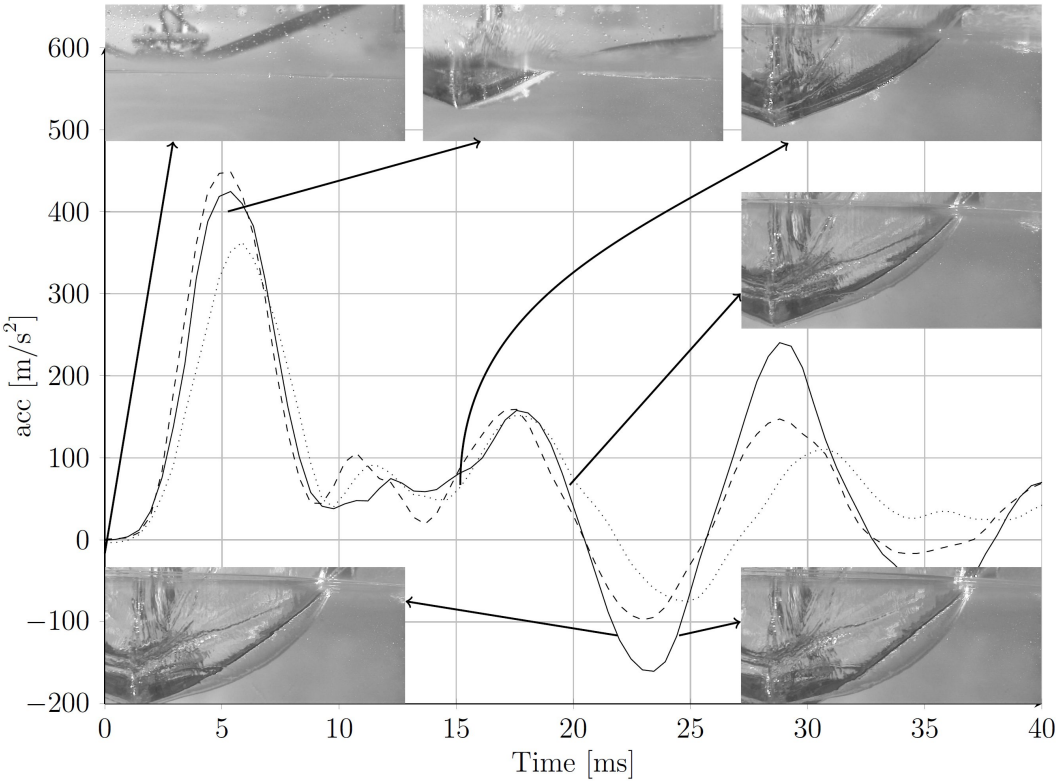


**Figure 14.** Graph of the recorded acceleration of a wedge (V, $\beta = 20°$, 2 mm thick) entering the water at 5.6 m/s and high speed camera images captured at 0, 5, 15, 20, 22.5, and 25 ms.

Figure 14 shows the time traces of acceleration recorded during the water entry of a composite wedge (V2) with $\beta = 20°$ entering the water at 5.6 m/s. Three repetitions of the same experiment are

Preprints (www.preprints.org) | NOT PEER-REVIEWED | Posted: 19 October 2018 doi:10.20944/preprints201810.0441.v1

Peer-reviewed version available at J. Mar. Sci. Eng. 2018, 6, 155; doi:10.3390/jmse6040155



shown (solid, dashed, and dotted lines). Images from the high speed camera at characteristic time instants of the impact are superimposed to the graph to get a better overview of the impact dynamics. Notably, the acceleration suddenly turns negative at about 20 ms from the impact (positive acceleration in the plot is opposite to gravity, and free fall is referenced as 0). Such behaviour is very uncommon in water entry, as it represents a body being sucked into the water. The analysis of the high speed images show that acceleration starts its decreasing trend to eventually attain negative values after the cavity is generated within the fluid. It was further found that acceleration turns positive as the cavity pockets collapse. Results thus evidence a strong relation between cavity evolution and impact dynamics.

## 6. Analysis of the fluid motion

The following section focuses on the evaluation of the fluid motion during the water entry, with particular interest on the instants of cavity formation. To this effort, a numerical model based on a coupled FEM/SPH scheme is utilized to gain further understanding of this peculiar FSI phenomenon.

The numerical solution bases on a coupled FEM-SPH technique, where the body is modeled with FEM elements and the fluid with the SPH particles. In-depth details about the implementation of the numerical scheme utilized here can be found in previous works by the authors [40,43] and are not reported here for brevity. The numerical scheme utilized herein is the same one described and validated in [40,43], and is here utilized to get further insights on the cavity formation phenomenon. The results presented in the following are mainly qualitative and are not intended to be a validation of the numerical model, as results are actually found to be faulty as soon as cavity is formed. It will be commented in the following that the numerical scheme utilized here can not capture the physics beneath the cavity formation process. Notwithstanding the incapability of the numerical scheme to capture this particular FSI phenomena, its results are helpful when trying understanding its onset.

An example of a numerical simulation is shown in figure 15. Similarly to the experimental observations, once the maximum concave deformation is reached (central-left image), a void with cylindrical wavefront is generated within the fluid. Results show that some portions of the panels with higher amplitude of vibration might have a vertical velocity component that differs (not only in magnitude but also in direction) from the local velocity of the fluid. There is therefore a tendency of the fluid to move away from the wedge generating a void, as shown in figure 16. The images show the vector-plots of the absolute velocity (left) and the vertical component only (right). Due to the structural vibration, after the maximum concave deflection is reached, the central portion of the wedge assumes an instantaneous upward velocity, whereby the fluid maintains its motion due to inertia. Therefore, the panel and the fluid beneath assume opposite directions, facilitating the cavity formation.

It thus appears that the wavefront observed during experiments is introduced by a local discontinuity between the wedge and the fluid vertical velocities. It is realistic to assume that this region will encounter an underpressure. However, the numerical model is not really capable of correctly modeling the cavity formation phenomenon. We must note that the present results highlights an important limitation of the coupled FEM/SPH model utilized here. In fact, the numerical model represents a 2D section of the wedge. Results from the simulation should be therefore valid only at the mid-span of the wedge, where the 2D approximation holds [44]. Therein, experimental findings do not show any fluid detachment from the wedge. The cavity pocket formation is instead originating only at the front and back sides of the wedge, where the water can not experience underpressure as it faces air. The numerical model can not efficiently treat the contact between the fluid and the structure, not being able to model the correct boundary condition for the fluid, which detaches from the structure instead of going under-pressure. As a result, the numerical model better describes the physics at the sides of the wedge rather than at its mid-span. However, in this vision, the model is neglecting 3D effects, which indeed are important in the proximity of the front and back sides [44–46]. The model can therefore be considered valid only until the cavity pocket formation onset.

Preprints (www.preprints.org) | NOT PEER-REVIEWED | Posted: 19 October 2018 doi:10.20944/preprints201810.0441.v1

Peer-reviewed version available at J. Mar. Sci. Eng. 2018, 6, 155; doi:10.3390/jmse6040155



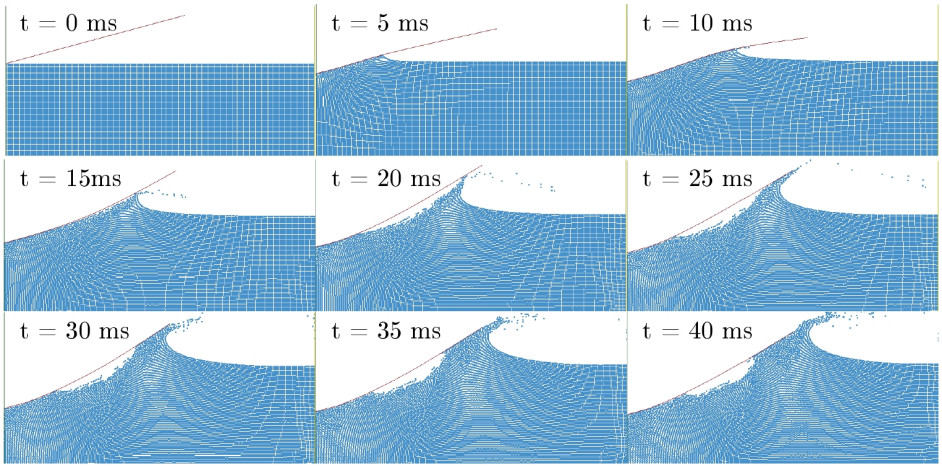


**Figure 15.** Numerical simulation of the water entry of an aluminium wedge 2 *mm* thick with deadrise angle of 15° entering the water at 4.2 m/s. Once the maximum concave deformation is reached (in the fourth image) a void with a cylindrical wavefront generates.

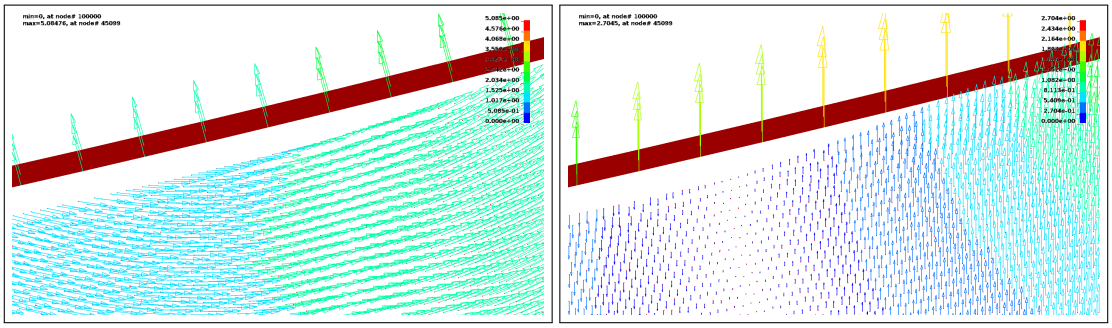

**Figure 16.** Velocities in the wedge and the fluid obtained from the numerical simulation. Absolute (left) and vertical component only (right).

## 7. Conclusions

Experimental drop-tests of flexible wedges were performed to study the Fluid-Structure Interaction phenomena that generate during the water entry, with particular attention to the cavity formation process and its effect on impact dynamics. It was found that when the deflection of the wedge is small, no fluid-structure interaction phenomena appear and established analytical formulations for rigid bodies can be used to evaluate the impact force and the hydrodynamic pressure. However, large structural deformations were found to have strong effects on the fluid motion. In particular, large deformations might introduce air pockets characterized by a cylindrical wavefront originating at the fluid/structure interface. Such cavity is found to equally originate from the front and rear faces of the structure, and their shape is not in line with the analytical predictions, as it seems not to originate from the keel, where pressure is supposed to be the lowest, but along the entire wet length of the structure. The cavity will eventually collapse during the water entry, and in the most severe impacts cases successive pockets (with decreasing amplitude) might generate and collapse repetitively. The pockets are found to increase with the impact velocity and the flexibility of the wedge. The largest cavities were further found to strongly affect the impact dynamics, up to the cases where the overall acceleration of the body turns negative within the timeframe between the cavity formation and its collapse.

Numerical simulations suggest that cavity formation is ruled by a differential between structure and fluid velocities introduced by structural vibrations. Results also highlight that the coupled

Preprints (www.preprints.org) | NOT PEER-REVIEWED | Posted: 19 October 2018 doi:10.20944/preprints201810.0441.v1

Peer-reviewed version available at J. Mar. Sci. Eng. 2018, 6, 155; doi:10.3390/jmse6040155



FEM/SPH numerical model utilized here, which actually suffers similar drawbacks of many other coupled numerical schemes utilized in the literature, is capable to predict the onset of cavity formation. However, it can not correctly predict its evolution due to a weak coupling between SPH particles and FEM elements, which can not fully treat the proper boundary condition for the fluid.

**Author Contributions:** Conceptualization, Giangiacomo Minak; Data curation, Riccardo Panciroli; Funding acquisition, Riccardo Panciroli and Giangiacomo Minak; Resources, Tiziano Pagliaroli; Supervision, Giangiacomo Minak; Visualization, Tiziano Pagliaroli; Writing – original draft, Riccardo Panciroli; Writing – review & editing, Tiziano Pagliaroli.

## References

1. Qin, Z.; Batra, R.C. Local slamming impact of sandwich composite hulls. *International Journal of Solids and Structures* **2009**, *46*, 2011–2035. doi:10.1016/j.ijsolstr.2008.04.019.
2. Carcaterra, A.; Ciappi, E. Prediction of the Compressible Stage Slamming Force on Rigid and Elastic Systems Impacting on the Water Surface. *Nonlinear Dynamics* **2000**, *21*, 193–220.
3. Carcaterra, A.; Ciappi, E. Hydrodynamic shock of elastic structures impacting on the water: theory and experiments. *Journal of Sound and Vibration* **2004**, *271*, 411–439. doi:10.1016/j.jsv.2003.02.005.
4. Panciroli, R.; Minak, G. Experimental evaluation of the air trapped during the water entry of flexible structures. *Acta Imeko* **2014**, *3*, 63–67.
5. Kapsenberg, G.K. Slamming of ships: where are we now? *Philosophical Transactions of the Royal Society A: Mathematical, Physical and Engineering Sciences* **2011**, *369*, 2892–2919. doi:10.1098/rsta.2011.0118.
6. Faltinsen, O.M. Hydroelastic slamming. *Journal of Marine Science and Technology* **2000**, *5*, 49–65. doi:10.1007/s007730070011.
7. Faltinsen, O.M.; Landrini, M.; Greco, M. Slamming in marine applications. *Journal of Engineering Mathematics* **2004**, *48*, 187–217. doi:10.1023/B:engi.0000018188.68304.ae.
8. Fragassa, C. Engineering Design Driven by Models and Measures: The Case of a Rigid Inflatable Boat **2018**. doi:10.20944/PREPRINTS201810.0131.V1.
9. Fragassa, C.; Minak, G. Measuring Deformations in a Rigid-Hulled Inflatable Boat. *Key Engineering Materials* **2017**, *754*, 295–298. doi:10.4028/www.scientific.net/KEM.754.295.
10. Seddon, C.; Moatamedi, M. Review of water entry with applications to aerospace structures. *International Journal of Impact Engineering* **2006**, *32*, 1045–1067. doi:10.1016/j.ijimpeng.2004.09.002.
11. Campbell, J.C.; Vignjevic, R. Simulating structural response to water impact. *International Journal of Impact Engineering* **2012**, *49*, 1–10. doi:10.1016/j.ijimpeng.2012.03.007.
12. Hughes, K.; Vignjevic, R.; Campbell, J.; De Vuyst, T.; Djordjevic, N.; Papagiannis, L. From aerospace to offshore: Bridging the numerical simulation gaps–Simulation advancements for fluid structure interaction problems. *International Journal of Impact Engineering* **2013**, *61*, 48–63. doi:10.1016/j.ijimpeng.2013.05.001.
13. Wagner, H. {Ü}ber Sto{ß}- und Gleitvorg{ä}nge an der Oberfl{ä}che von Fl{ü}ssigkeiten. *ZAMM - Zeitschrift f{ü}r Angewandte Mathematik und Mechanik* **1932**, *12*, 193–215. doi:10.1002/zamm.19320120402.
14. Chuang, S.L. Investigation of impact of rigid and elastic bodies with water. *NSRDC report no. 3248* **1970**.
15. Panciroli, R.; Porfiri, M. Evaluation of the pressure field on a rigid body entering a quiescent fluid through particle image velocimetry. *Experiments in Fluids* **2013**, *54*, 1630. doi:10.1007/s00348-013-1630-3.
16. Korobkin, A.; Parau, E.I.; Vanden-Broeck, J.M. The mathematical challenges and modelling of hydroelasticity. *Philosophical transactions. Series A, Mathematical, physical, and engineering sciences* **2011**, *369*, 2803–2812. doi:10.1098/rsta.2011.0116.
17. Korobkin, A.; Guéret, R.; Malenica, Š. Hydroelastic coupling of beam finite element model with Wagner theory of water impact. *Journal of Fluids and Structures* **2006**, *22*, 493–504. doi:10.1016/j.jfluidstructs.2006.01.001.
18. Das, K.; Batra, R.C. Local water slamming impact on sandwich composite hulls. *Journal of Fluids and Structures* **2011**, *27*, 523–551. doi:10.1016/j.jfluidstructs.2011.02.001.
19. Zhao, R.; Faltinsen, O.; Aarsnes, J. Water entry of Arbitrary Two-Dimensional sections with and without flow separation. Twenty-First Symposium on Naval Hydrodynamics, 1997.
20. Scolan, Y. Hydroelastic behaviour of a conical shell impacting on a quiescent-free surface of an incompressible liquid. *Journal of Sound and Vibration* **2004**, *277*, 163–203. doi:10.1016/j.jsv.2003.08.051.

Preprints (www.preprints.org) | NOT PEER-REVIEWED | Posted: 19 October 2018 doi:10.20944/preprints201810.0441.v1

Peer-reviewed version available at J. Mar. Sci. Eng. 2018, 6, 155; doi:10.3390/jmse6040155




21. Wu, G.X.; Sun, H.; He, Y.S. Numerical simulation and experimental study of water entry of a wedge in free fall motion. *Journal of Fluids and Structures* **2004**, *19*, 277–289. doi:10.1016/j.jfluidstructs.2004.01.001.
22. Von Karman, T. The impact on seaplane floats, during landing. *NACA-TN-321* **1929**.
23. Backer, G.D.; Vantorre, M.; Beels, C.; Pré, J.D.; Victor, S.; Rouck, J.D.; Blommaert, C.; De Backer, G.; Vantorre, M.; Beels, C.; De Pré, J.; Victor, S.; De Rouck, J.; Blommaert, C.; Van Paepegem, W. Experimental investigation of water impact on axisymmetric bodies. *Applied Ocean Research* **2009**, *31*, 143–156. doi:10.1016/j.apor.2009.07.003.
24. El Malki Alaoui, A.; Nême, A.; Tassin, A.; Jacques, N.; Alaoui, A.E.M.; Nême, A.; Tassin, A.; Jacques, N. Experimental study of coefficients during vertical water entry of axisymmetric rigid shapes at constant speeds. *Applied Ocean Research* **2012**, *37*, 183–197. doi:10.1016/j.apor.2012.05.007.
25. Chuang, S.L.; Milne, D.T. Drop tests of cone to investigate the three-dimensional effect of slamming. *NRDC report no. 3543* **1971**.
26. Korobkin, A. Cavitation in liquid impact problems. Fifth International Symposium on Cavitation ( CAV2003 ); , 2003; Vol. 2, pp. 1–7.
27. Faltinsen, O.M. The effect of hydroelasticity on ship slamming. *Philosophical Transactions of the Royal Society A: Mathematical, Physical and Engineering Sciences* **1997**, *355*, 575–591. doi:10.1098/rsta.1997.0026.
28. Reinhard, M.; Korobkin, a.a.; Cooker, M.J. Cavity formation on the surface of a body entering water with deceleration. *Journal of Engineering Mathematics* **2015**. doi:10.1007/s10665-015-9788-8.
29. Bivin, Y.K.; Glukhov, Y.M.; Permyakov, Y.V. Vertical entry of solids into water. *Fluid Dynamics* **1986**, *20*, 835–841. doi:10.1007/BF01049923.
30. Yadong, W.; Xulong, Y.; Yuwen, Z. Natural Cavitation in High Speed Water Entry Process. Proceedings of the 1st International Conference on Mechanical Engineering and Material Science; Atlantis Press: Paris, France, 2012; Number Mems, pp. 46–49. doi:10.2991/mems.2012.18.
31. Korobkin, A.A.; Khabakhpasheva, T.I.; Wu, G.X. Coupled hydrodynamic and structural analysis of compressible jet impact onto elastic panels. *Journal of Fluids and Structures* **2008**, *24*, 1021–1041. doi:10.1016/j.jfluidstructs.2008.03.002.
32. Korobkin, A.; Ellis, A.S.; Smith, F.T. Trapping of air in impact between a body and shallow water. *Journal of Fluid Mechanics* **2008**, *611*, 365–394. doi:10.1017/S0022112008002899.
33. Hicks, P.D.; Ermanyuk, E.V.; Gavrilov, N.V.; Purvis, R.; Mechanics, F. Air trapping at impact of a rigid sphere onto a liquid. *Journal of Fluid Mechanics* **2012**, *695*, 310–320. doi:dx.doi.org/10.1017/jfm.2012.20.
34. Cuomo, G.; Piscopia, R.; Allsop, W. Evaluation of wave impact loads on caisson breakwaters based on joint probability of impact maxima and rise times. *Coastal Engineering* **2011**, *58*, 9–27. doi:10.1016/j.coastaleng.2010.08.003.
35. Panciroli, R.; Porfiri, M. Hydroelastic impact of piezoelectric structures. *International Journal of Impact Engineering* **2014**, *66*, 18–27. doi:10.1016/j.ijimpeng.2013.12.007.
36. Jalalisendi, M.; Porfiri, M. Water entry of compliant slender bodies: Theory and experiments. *International Journal of Mechanical Sciences* **2017**, *000*, 1–16. doi:10.1016/j.ijmecsci.2017.07.041.
37. Panciroli, R.; Porfiri, M. Analysis of hydroelastic slamming through particle image velocimetry. *Journal of Sound and Vibration* **2015**, *347*, 63–78. doi:10.1016/j.jsv.2015.02.007.
38. Shams, A.; Zhao, S.; Porfiri, M. Water impact of syntactic foams. *Materials* **2017**, *10*. doi:10.3390/ma10030224.
39. Mei, R.; Luo, L.S.; Shyy, W. An Accurate Curved Boundary Treatment in the Lattice {{}B{}}oltzmann Method. *Journal of Computational Physics* **1999**, *155*, 307–330.
40. Panciroli, R.; Abrate, S.; Minak, G.; Zucchelli, A. Hydroelasticity in water-entry problems: Comparison between experimental and SPH results. *Composite Structures* **2012**, *94*, 532–539. doi:10.1016/j.compstruct.2011.08.016.
41. Panciroli, R.; Abrate, S.; Minak, G. Dynamic response of flexible wedges entering the water. *Composite Structures* **2013**, *99*, 163–171. doi:10.1016/j.compstruct.2012.11.042.
42. Panciroli, R. Hydroelastic impacts of deformable wedges. PhD thesis, Alma Mater Studiorum Università di Bologna, 2012. doi:10.6092/unibo/amsdottorato/4594.
43. Panciroli, R. Hydroelastic Impacts of Deformable Wedges. In *Solid Mechanics and its Applications*; Abrate, S.; Castanié, B.; Rajapakse, Y.D.S., Eds.; Springer Netherlands: Dordrecht, 2013; Vol. 192, *Solid Mechanics and Its Applications*, pp. 1–45. doi:10.1007/978-94-007-5329-7_1.

Preprints (www.preprints.org) | NOT PEER-REVIEWED | Posted: 19 October 2018 doi:10.20944/preprints201810.0441.v1

Peer-reviewed version available at J. Mar. Sci. Eng. 2018, 6, 155; doi:10.3390/jmse6040155




44. Jalalisendi, M.; Shams, A.; Panciroli, R.; Porfiri, M. Experimental reconstruction of three-dimensional hydrodynamic loading in water entry problems through particle image velocimetry. *Experiments in Fluids* **2015**, *56*, 1–17. doi:10.1007/s00348-015-1895-9.
45. Yu, P.; Ong, M.; Li, H. Effects of Added Mass and Structural Damping on Dynamic Responses of a 3D Wedge Impacting on Water. *Applied Sciences* **2018**, *8*, 802. doi:10.3390/app8050802.
46. Jalalisendi, M.; Osma, S.J.; Porfiri, M. Three-dimensional water entry of a solid body: A particle image velocimetry study. *Journal of Fluids and Structures* **2015**, *59*, 85–102. doi:10.1016/j.jfluidstructs.2015.08.013.